Journal of NUCLEAR SCIENCE and TECHNOLOGY, Vol. 46, No. 6, p. 613–623 (2009)

ARTICLE

Computational Methodology of Sodium-Water Reaction Phenomenon in Steam Generator of Sodium-Cooled Fast Reactor

Takashi TAKATA[1,*], Akira YAMAGUCHI[1], Akihiro UCHIBORI[2] and Hiroyuki OHSHIMA[2]

[1]*Osaka University, Suita, Osaka 565-0871, Japan*
[2]*Japan Atomic Energy Agency, Narita, O-arai-machi, Ibaraki 311-1393, Japan*

(Received May 27, 2008 and accepted in revised form March 4, 2009)

A new computational methodology of sodium-water reaction (SWR), which occurs in a steam generator of a liquid-sodium-cooled fast reactor when a heat transfer tube in the steam generator fails, has been developed considering multidimensional and multiphysics thermal hydraulics. Two kinds of reaction models are proposed in accordance with a phase of sodium as a reactant. One is the surface reaction model in which water vapor reacts directly with liquid sodium at the interface between the liquid sodium and the water vapor. The reaction heat will lead to a vigorous evaporation of liquid sodium, resulting in a reaction of gas-phase sodium. This is designated as the gas-phase reaction model. These two models are coupled with a multidimensional, multicomponent gas, and multiphase thermal hydraulics simulation method with compressibility (named the 'SERAPHIM' code). Using the present methodology, a numerical investigation of the SWR under a pin-bundle configuration (a benchmark analysis of the SWAT-1R experiment) has been carried out. As a result, the maximum gas temperature of approximately 1,300°C is predicted stably, which lies within the range of previous experimental observations. It is also demonstrated that the maximum temperature of the mass weighted average in the analysis agrees reasonably well with the experimental result measured by thermocouples. The present methodology will be promising to establish a theoretical and mechanical modeling of secondary failure propagation of heat transfer tubes due to such as an overheating rupture and a wastage.

KEYWORDS: computational fluid dynamics, sodium-water reaction, multiphase analysis, steam generator, sodium-cooled fast reactor

I. Introduction

In a steam generator of a sodium-cooled fast reactor, water and/or water vapor flows inside the heat transfer tubes and liquid sodium flows in the shell side. Inside the heat transfer tubes, the water and/or water vapor is highly pressurized to enhance the power generation efficiency. On the other hand, the pressure load of the liquid sodium is only a few times as high as atmospheric pressure because of the high boiling point of liquid sodium (881°C at atmospheric pressure). Accordingly, the water and/or water vapor will leak into the liquid sodium and a sodium-water reaction (SWR) will take place at the shell side of the steam generator when a heat transfer tube fails.

The initial stage of the leakage can be classified into several categories,[1)] depending on the leakage rate, such as 'microleak,' 'small leak,' 'intermediate leak,' and 'large leak.' When a very small leak (<50 mg/s; 'microleak') takes place, the structure of the adjacent heat transfer tube is not affected by the leak. Instead, the deterioration of mechanical strength occurs at the site of the initial defect. It is experimentally observed that plugging and peeling of sodium compounds occur at the defect.[2)] As a result, the defect can eventually enlarge to a size that allows a stable reacting jet[3)] and the defect will be characterized as a 'small leak (<10 g/s)' and 'intermediate leak (<2 kg/s).' Under the 'small leak' condition, the deterioration of mechanical strength at a high temperature (designated as an overheating rupture) and/or high alkali corrosion-erosion (designated as a wastage) will occur continuously at the surface of the adjacent heat transfer tube. Consequently, a secondary tube failure may occur when a monitoring system fails to detect leakage, resulting in larger leakage characteristics of 'intermediate leak' or 'large leak (>2 kg/s).' The prevention and/or the prediction of secondary tube failure due to overheating rupture and wastage is one of the key issues of structural integrity in the system.

In the wastage and the overheating rupture phenomena, local characteristics of the reaction zone, such as temperature, void fraction, and components of gas, near the target play important roles. However, it is not easy to measure such characteristics because of the high-temperature, high-velocity, and strongly alkaline environment in the reacting zone. Hence, the prediction of the wastage and the rupture was arranged based not on the local characteristics but on a

*Corresponding author, E-mail: takata_t@see.eng.osaka-u.ac.jp

representative characteristic in the previous works. For instance, the following correlation was evolved for $2\frac{1}{4}$Cr-1Mo steel with $25 < L/D < 150$:[1)]

$$W_R = \frac{4400}{L}\exp\left\{-\left[0.255\left(\ln\frac{G}{5.12}\right)^2\right]+\frac{5460}{T_S}\right\}, \quad (1)$$

where W_R, L, G, and T_S are the wastage rate, the distance between the leakage and target, the leakage rate, and the sodium temperature, respectively. In the case of the overheating rupture phenomenon, the deterioration of tube material is assessed numerically, taking into account heat flux on the outer surface of the tube, based on a conservative fluid temperature and a heat transfer coefficient obtained from experimental results.[4)]

A numerical simulation of the SWR is an alternative way to investigate the local characteristics close to heat transfer tubes adjoining the failure tube in order to evaluate the wastage rate and the probability of overheating rupture in detail. For this purpose, several multidimensional simulation methods were developed in previous works, such as 'LEAP-JET'[5)] and 'SHAMPAGNE.'[6)] However, an empirical reaction model of the SWR, which represents a maximum temperature similar to the experimental results using a tuning factor, was implemented in those methods. Hence, a mechanistic and theoretical modeling of the SWR and a multiphysics computational tool of thermal hydraulics are needed to assess the SWR phenomenon. For this purpose, the authors have developed a new computational methodology of the SWR[7–9)] (named the 'SERAPHIM' code).

In the present paper, the benchmark analysis of the SWAT-1R experiment,[10)] in which an intermediate leakage (approximately 0.16 kg/s) was observed under a pin bundle configuration by measuring mainly temperature, has been carried out to examine the applicability of the developed methodology to the SWR phenomenon under the complicated geometrical configuration. Furthermore, characteristics of the reacting zone, such as the volume fraction of gas, temperature in each phase, and mass concentration of sodium compounds, have also been investigated numerically.

II. Computational Methodology of Sodium-Water Reaction

In a numerical analysis, one has to choose an appropriate numerical model for the subject of research. The subject of the present research is the investigation of the characteristics of the reacting zone and the influence on neighbor heat transfer tubes in the SWR phenomena numerically. The approach of a homogenous model with continuum approximation by the surface tracking method is too precise for this purpose in spite of the current striking progress of computer speed. On the other hand, simple models such as a homogeneous fluid model, a slip model, and a drift flux model for multiphase analysis cannot depict the phenomena. Accordingly, a multifluid model with one pressure is applied in the present methodology. In a multifluid model, the governing equations of each phase are taken into consideration separately. The information of the gas-liquid interface is described as an interfacial area density that is determined by a constitutive equation.

1. Numerical Investigation of Reaction Mechanism

In a faithful numerical investigation of the SWR phenomenon, a chemical reaction process at the reacting zone should be clarified carefully. From the experimental observation,[11)] in which a residue a long time after the SWR was inspected, it was found that sodium hydroxide (NaOH), sodium oxide (Na_2O), and sodium hydride (NaH) were the dominant sodium compounds in the chemical process. However, sodium hydride is unstable under a high-temperature configuration like that in the reacting zone. Hence, it was likely that sodium hydride would be produced not in the reacting zone but in the remaining liquid sodium in the test apparatus during its cooling after the experiment. In another previous work,[12)] it was reported that the SWR could be divided into two stages: at the first stage, sodium hydroxide is produced dominantly, and at the second stage, the chemical interaction of products from the first stage (sodium hydroxide and hydrogen gas) takes place to produce sodium oxide and hydride under an excessive sodium condition. Furthermore, in the numerical investigation of the theoretical adiabatic flame temperature of the SWR,[13)] it was found that sodium hydroxide in both gas and liquid phases would be the dominant sodium compound.

As mentioned above, the mechanism of the SWR is not fully understood, especially in the reacting zone. Consequently, the authors investigated the reaction mechanism and its reaction path using an *ab initio* molecular orbital (MO) method[8)] and the following knowledge was obtained. Firstly, the energy barrier in producing sodium oxide (327 kJ/mol) is quite high compared with that in the sodium hydroxide process (201 kJ/mol). The energy barrier is needed to generate a reactant product (to complete the reaction). Hence, when the energy barrier becomes smaller, the probability of the reaction becomes higher, resulting in a higher reaction rate. Thus, sodium hydroxide will be a dominant reactant product in the reacting zone. The reaction rate of both sodium hydroxide and sodium oxide will be discussed later.

Secondly, it was found that all of the SWRs are endothermic in the gas phase when hydrogen exists as a monoatom. This leads to the fact that an additional energy is necessary to initiate the SWR. It was also found that only the hydration of sodium is exothermic in the MO investigation. Consequently, the hydration of sodium might be a key phenomenon in initiating the SWR. It is carefully noted that the latent heat of the reactant products from the gas phase to liquid and/or solid phases and the reaction heat of hydrogen gas generation turn the endothermic reactions into exothermic ones.

From the comparison of the energy barrier mentioned above and the previous works of the two-stage reaction process and the adiabatic temperature investigation, it is an appropriate assumption that the following reaction is dominant in the reacting zone in the SWR.

$$Na + H_2O \rightarrow NaOH + 1/2H_2 \quad (2)$$

2. Reaction Models

When water leaks into liquid sodium in the steam generator, it will evaporate immediately due to depressurization. In addition, the interface between water and liquid sodium will be covered with hydrogen gas instantaneously even if the water reacts with the liquid sodium directly. Accordingly, it will be appropriate that the liquid sodium is in contact with the water vapor dominantly during the SWR. On the contrary, the liquid sodium will be vaporized because of the reaction heat at a later stage of the SWR phenomenon. Consequently, the reaction models in which the water vapor reacts with both liquid and gas-phase sodium have been implemented in the SERAPHIM code.

(1) Surface Reaction

When the liquid sodium reacts with water vapor, an analogy between heat and mass transfer is applied.[7] This reaction is designated as the surface reaction model. If the water vapor diminishes at the liquid sodium surface, the mass flow rate of the water vapor ($\gamma^{sf}_{H_2O}$) toward the liquid surface is expressed as

$$\gamma^{sf}_{H_2O} = -Le^{b-1} a \frac{H_g}{Cp_g} Y_{H_2O}. \tag{3}$$

Here, Le, a, H, Cp, and Y mean the Lewis number, the interfacial area density, the heat, transfer coefficient, the specific heat, and the mass fraction, respectively. b is the empirical parameter. The superscript sf means the surface reaction and the subscripts g and H_2O represent the gas phase and the water vapor.

The heat transfer coefficient (H_g) in Eq. (3) is determined to be approximately 10,000 $\mathrm{W/m^2/K}$ based on the results of an experiment[14] in which the heat transfer coefficient on the surface of a heat transfer tube at the reacting zone was measured under the SWR situation. The Lewis number varies quickly from 0.2 to 1.7 in the SWR phenomenon corresponding to the concentrations of water vapor and hydrogen gas. The empirical constant b becomes less than unity from the viewpoint of previous experimental heat transfer correlations in the turbulent state. In the present study, b is set to 0 so that one obtains a maximum reaction rate at the lowest Lewis number. It is noted that the empirical constant b is not so influential on the reacting zone.[15] When the reaction rate of water vapor is evaluated from Eq. (3), the reaction rates of the liquid sodium and the reaction product are calculated from the stoichiometric coefficient (i_{st}). In the present paper, only sodium hydroxide is assumed as the sodium compound in the SWR and the stoichiometric coefficient is determined using Eq. (2):

$$\gamma^{sf}_j = i_{st\,j} \gamma^{sf}_{H_2O}, \tag{4}$$

$$i_{st\,Na} = \frac{M_{Na}}{M_{H_2O}},\ i_{st\,NaOH} = -\frac{M_{NaOH}}{M_{H_2O}},\ i_{st\,H_2} = -\frac{M_{H_2}}{2M_{H_2O}}. \tag{5}$$

Here, M is the molar weight.

(2) Gas-Phase Reaction

With regard to the gas-phase reaction, a well-known rate equation is applied to evaluate the reaction rate as follows:

$$\gamma^{gs}_A = mM_A k(T)[A]^m[B]^n. \tag{6}$$

Here, $k(T)$ is the rate constant. $[A]$ and $[B]$ mean the molar concentrations of reactants A and B. The powers m and n indicate the number of reactants in the chemical formula. The superscript gs means the gas-phase reaction. The rate constant has been evaluated based on the MO investigation.[8] The transient state theory[16] or the capture theory[17] are applied to describe the rate constant in the form of the Arrhenius law depending on the existence of the transient state during the reaction path.

Table 1 Rate constant in gas-phase model

Rate constant $k(T)$ [mol, m, s]	Temperature [°C]		
	500	1,000	1,500
Eq. (2) (NaOH)	2.97×10^{-7}	1.12×10^{-1}	3.35×10^{1}
Eq. (7) (Na_2O)	3.65×10^{-17}	2.80×10^{-8}	2.44×10^{-4}

Let us discuss the reaction rates of both processes of sodium hydroxide and oxide generation briefly. For sodium hydroxide generation, the irreversible reaction shown in Eq. (2) is estimated. The following chemical formula is applied for the sodium oxide process.

$$2\mathrm{Na} + \mathrm{H_2O} \rightarrow \mathrm{Na_2O} + \mathrm{H_2} \tag{7}$$

From the transient state theory and the capture theory, each rate constant has been estimated as[8]

$$\begin{aligned} k(T)_{\mathrm{Eq.(2)}} &= 4.43 \times 10^4 T^{0.88} \exp\left(-\frac{2.03 \times 10^5}{RT}\right), \\ k(T)_{\mathrm{Eq.(7)}} &= 4.09 \times 10^1 T^{1.33} \exp\left(-\frac{3.24 \times 10^5}{RT}\right). \end{aligned} \tag{8}$$

Here, R is the gas constant. **Table 1** summarizes the rate constants at a typical temperature, calculated from Eq. (8). It is again demonstrated that sodium hydroxide is the dominant species in the reaction zone of the SWR.

3. Thermal-Hydraulic Model in SERAPHIM

Two liquid phases of sodium and water and one multicomponent gas phase are taken into account as a working fluid. It is assumed that all reaction products of the surface reaction and the gas-phase reaction are emitted to the gas phase. Hence, water vapor, sodium vapor, hydrogen, and sodium hydroxide of both liquid and gas phases are considered as gas species.

As an example, governing equations of the gas phase mass, momentum, and energy are written, respectively, as

$$\begin{aligned} &\frac{\partial}{\partial t}(\alpha_g \rho_g) + \nabla \cdot (\alpha_g \rho_g \mathbf{u}_g) \\ &\quad = \Gamma^e_H - \Gamma^c_H + \Gamma^e_S - \Gamma^c_S + G^{sf} + G^{dif}, \end{aligned} \tag{9}$$

$$\begin{aligned} &\frac{\partial}{\partial t}(\alpha_g \rho_g \mathbf{u}_g) + \nabla \cdot (\alpha_g \rho_g \mathbf{u}_g \mathbf{u}_g) \\ &\quad = -\alpha_g \nabla p + \alpha_g \nabla \cdot \tau_g + \alpha_g (\rho_g - \rho_0)\mathbf{g}, \\ &\qquad + \Gamma^e_S \mathbf{u}_S - \Gamma^c_S \mathbf{u}_g + \Gamma^e_H \mathbf{u}_H - \Gamma^c_H \mathbf{u}_g, \\ &\qquad - f^{ph}_S (\mathbf{u}_g - \mathbf{u}_S) - f^{ph}_H (\mathbf{u}_g - \mathbf{u}_H), \\ &\qquad - G^{sf} (\mathbf{u}_g - \mathbf{u}_S), \\ &\qquad - f^w_g \mathbf{u}_g; \end{aligned} \tag{10}$$

$$\frac{\partial}{\partial t}(\alpha_g \rho_g h_g) + \nabla \cdot (\alpha_g \rho_g h_g \mathbf{u}_g)$$
$$= \alpha_g \frac{D}{Dt} p + \alpha_g \Phi_g + \alpha_g \nabla \cdot (\lambda_g \nabla T_g),$$
$$+ \Gamma^e_S (h_S + i_S) - \Gamma^c_S h y_{Na} + \Gamma^e_H (h_H + i_H) - \Gamma^c_H h y_{H_2O},$$
$$- \alpha_g H_S (T_g - T_S) - \alpha_g H_H (T_g - T_H),$$
$$+ S^{sf} + S^{gs},$$
$$- \alpha_g H^w_g (T_g - T_w) + S^{dif}, \qquad (11)$$

$$\left(\frac{D}{Dt} = \frac{\partial}{\partial t} + \mathbf{u}_G \cdot \nabla \right),$$

where α, ρ, t, $\mathbf{u}$, Γ^e, and Γ^c are the volume fraction, the density, the time, the velocity vector, the evaporation rate, and the condensation rate, respectively. p, $\boldsymbol{\tau}$, $\mathbf{g}$, f^{ph}, and f^w mean the kinetic pressure, the viscous stress tensor, the gravity vector, the interfacial friction coefficient, and the friction coefficient on a wall. h, Φ, i, and hy are the enthalpy, the dissipation function, the latent heat, and the enthalpy of gas component. G and S are source terms of the mass and energy, respectively. Subscripts S and H mean the liquid sodium phase and the liquid phase of water, respectively. Superscript *dif* indicates an additional source term due to the Dufour effect in which mass and energy are transferred by a diffusion of gas species.

In the momentum and energy equations (Eqs. (10) and (11)), common terms such as pressure, diffusivity, and gravity are described in the first row on the right side of each equation. The second and third rows in Eqs. (10) and (11) represent the influence of evaporation and/or condensation and the interaction between liquid and gas phases, respectively. The fourth row of the equations indicates the additional terms due to the SWR. Other additional terms such as an interaction with walls and the Dufour effect are summarized in the last row in the equations.

Since water and/or water vapor is highly pressurized (approximately a hundred and several tens of times as high as atmospheric pressure), compressibility is needed especially in the gas phase. Therefore, the modified Benedict-Webb Rubin equation[18] is applied as an equation of state (EOS) in the gas phase.[19]

With regard to the constitutive equations that compensate the lack of equations for unknown variables in a multifluid model, the Nigmatulin model,[20] the Autruffe model,[21] the Silver-Simpson model,[22] and the Martinelli-Nelson model[23] are implemented for the interfacial area density (a), the phase friction factor (f^{ph}), the evaporation and/or condensation rate (Γ), and the wall friction factor (f^w), respectively.

As shown in Eqs. (10) and (11), no turbulent model is implemented in SERAPHIM currently. In the numerical investigation of the SWR at a pin bundle configuration, the mesh arrangement and time marching are comparatively fine (less than several mm and 10^{-6} s order). Hence, the turbulent state in each phase is calculated directly (a concept of MILES[24] is adopted.). On the contrary, the resolution of the interface between liquid and gas phases seems to be coarse. Consequently, the effect of turbulence is taken into consideration in terms of the heat transfer coefficient between liquid and gas phases and the surface reaction rate. With regard to the numerical solution, the HSMAC method considered with compressibility is applied.[7]

III. Numerical Investigation under a Pin-Bundle Configuration

In order to investigate the applicability of the present methodology on the actual SWR phenomenon in a steam generator and the influence of the reacting zone on neighbor tubes, a benchmark analysis of the SWAT-1R experiment[25] has been carried out. In this chapter, a summary of the SWAT-1R experiment is described first. Then the computational condition and the results of the numerical investigation are discussed.

1. SWAT-1R Experiment

Figure 1 shows the test apparatus of the SWAT-1R. The test apparatus consists of a double cylindrical vessel. In the experiment, liquid sodium was fed from the bottom of the outer vessel and also fed into the inner vessel through three holes placed at the bottom of the inner vessel, as shown in Fig. 1. Argon gas was put into the upper side of the test apparatus so as to suppress a pressure increase during the experiment. No forced convection was embedded to the liquid sodium in the experiment. The target leakage rate was set to 0.15 kg/s ('intermediate leak' category).

Inside the inner vessel, a pin bundle of 43 straight tubes, the alignment of which was the same as that of the Japanese prototype fast breeder reactor 'Monju' but rotated by an angle of 24°, was implemented. **Figure 2** depicts the test section of the pin bundle. An opening of ϕ 3.7 mm was placed on the upper side of one tube located at the bottom end of the bundle (gray tube in Fig. 2) and water vapor of

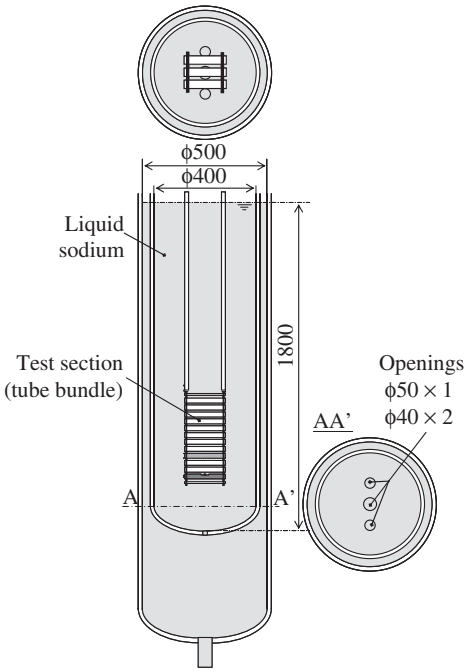

Fig. 1 Test apparatus of SWAT-1R

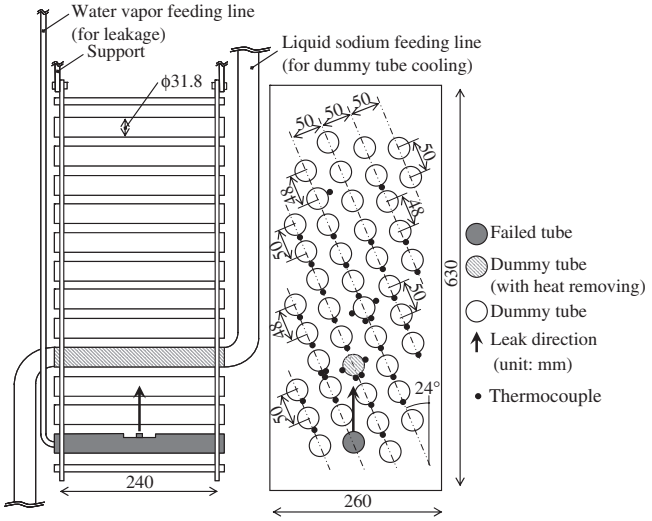

Fig. 2 Test section (pin bundle)

approximately 17.0 MPa and 352°C was blown vertically upward from the leakage.

A dozen thermocouples were installed at a certain place and temperature was measured mainly during the experiment in order to observe the temperature distribution in the reacting zone. In addition, some thermocouples were implanted into tubes adjacent to the leakage so that the heat transfer coefficients on the tube outer surface under the SWR configuration were evaluated. A flow of liquid sodium was provided inside one tube (hatched tube in Fig. 2) during the experiment in order to reproduce the heat exchange with water in the actual system. Both ends of the other tubes were opened and liquid sodium was supplied through the openings.

It is noted that the skewed bundle configuration was adopted in the experiment because of the spatial limitation in the test section. The angle of 24° was chosen so as to maximize the influence of the reacting zone on the neighboring tubes based on the previous observation.[26] The actual image of the leakage direction is indicated in **Fig. 3**.

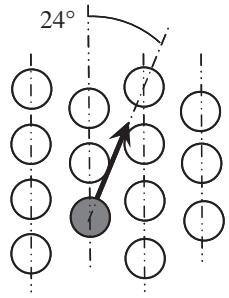

Fig. 3 Actual image of leakage direction

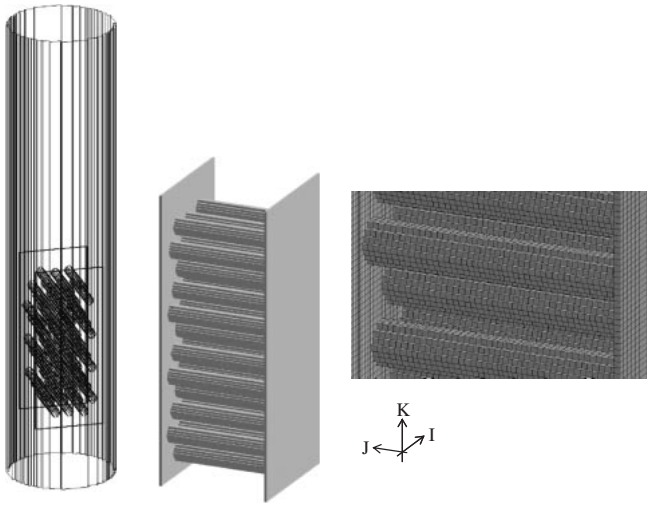

Fig. 4 Analytical geometry and mesh arrangement

2. Computational Condition

In the computation, the inside of the inner vessel from the bottom of the vessel, including three holes, to the liquid sodium surface is selected as the analytical region. Hence, the size of the analytical region is 400 mm in diameter and 1,800 mm in height (see Fig. 1). The structural mesh with the Cartesian coordinates is adopted and is divided into 122 (I) × 63 (J) × 172 (K), as shown in **Fig. 4**. The total number of meshes is approximately 1.3 million.

As the boundary condition, the constant pressure condition is applied to both leakage and the upper end boundary that corresponds to the liquid sodium surface. Hence, leakage rate is computed by solving the governing equations of the mass, the momentum, and the energy at the boundary.

Since the bottom end boundary (three holes) is placed comparatively near the leakage and it is expected that liquid sodium will flow into the analytical region through the boundary, a continuity of the pressure gradient ($\partial^2 P/\partial z^2 = 0$) is assumed. With regard to the thermal boundary condition, an adiabatic condition is assumed for simplicity. Hence, the heat capacity of the inner structure and the heat removal from the tubes are ignored in the analysis.

As mentioned in Sec. II-1, only sodium hydroxide is assumed as the sodium compound in the analysis. It is noted that the boiling point of sodium hydroxide is 1,390°C at atmospheric pressure and lies in a similar range to the maximum temperature observed in previous experimental research.[2,12] Furthermore, the latent heat of sodium hydroxide evaporation is considerably high compared with the reaction heat, as shown in the following:[27]

$$\mathrm{Na}(l) + \mathrm{H_2O}(g) \rightarrow \mathrm{NaOH}(l) + 1/2\mathrm{H_2}, \quad \Delta H^0_{298} = -177.46\,\mathrm{kJ/mol}. \tag{12}$$

$$\mathrm{NaOH}(l) \rightarrow \mathrm{NaOH}(g), \ \Delta H^0_{298} = 219.12\,\mathrm{kJ/mol}. \tag{13}$$

Here, (l) and (g) represent the liquid and gas phases. $\Delta H^0{}_{298}$ is the standard enthalpy change of formation and a negative value means exothermic. As shown in Eqs. (12) and (13), it is expected that a small amount of sodium hydroxide evaporation can affect the maximum temperature. Consequently, sodium hydroxide of both liquid and gas phases is considered in the analysis. An equivalent state assumption, where a proportion of the liquid and gas phases is determined from a saturation pressure profile, is adopted[9] to obtain an evaporation rate of sodium hydroxide.

Table 2 Computational condition

• **Initial conditions**	
[Water vapor]	
Temperature	: 352 [°C]
Pressure at the leakage	: 17.0 [MPa]
Leakage size	: 3.3 × 3.3 [mm]
(same area with experiment [ϕ3.7 mm])	
[Sodium]	
Temperature	: 470 [°C]
Initial pressure	: 0.2 [MPa]
• **Analytical conditions**	
Mesh arrangement	: 122 × 63 × 172
Time step	: 1.0 [μs]
Analysis time	: 0.6 [s]
Sodium compounds in the surface reaction	: NaOH (*g*) and (*l*)

In the authors' previous numerical investigation,[8] it was demonstrated that the surface reaction is much more intense than the gas-phase reaction. Moreover, gas-phase sodium appears downstream of the reacting zone in which almost all water vapor vanishes due to the reaction in the case of 'intermediate leakage.' Therefore, only the surface reaction is taken into consideration in the analysis.

The time step and the computation duration are set to 1.0 μs and 0.6 s respectively. The computational conditions are summarized in **Table 2**.

3. Results and Discussion

The spatial distributions of the gas volume fraction (void fraction) and the gas temperature at (a) 10 ms, (b) 100 ms (0.1 s), and (c) 600 ms (0.6 s) are shown in **Figs. 5** and **6**, respectively. It is noted that the region where the void fraction is larger than 0.1 is pictured as a colored contour in the following figures. The contours at the upper right of the figure indicate the cross section in accordance with J-K and I-K coordinates at the center. The contour at the bottom right shows the cross-sectional view of the I-J direction at 3 mm above the leakage (see Figs. 5(a) and 6(a)).

As in Fig. 5(a), the gas region develops spherically at the beginning of the leakage. Then, it develops along the inline (dashed-double-dotted line in Fig. 2) and the axial directions, as seen in Figs. 5(b) and 5(c). At the end of the analysis (at 0.6 s, Fig. 5(c)), the gas region almost covers up the gap space of the bundle. At that time, the gas flows out from the bundle through the inline direction. This is attributed to the fact that the flow resistance in the inline direction is lower than those in other directions. The white region, seen just above the upper end of the bundle in Fig. 5(c), means that liquid sodium is not swept out well because of the gas flow pattern.

It is noted that the leakage rate in the analysis becomes constant immediately because the pressure of 17.0 MPa at the leakage is set to be constant during the computation. On the other hand, a long and narrow feeding tube was implemented in the experiment (see Fig. 2). Therefore, the pressure at the leakage decreased rapidly and then returned to the

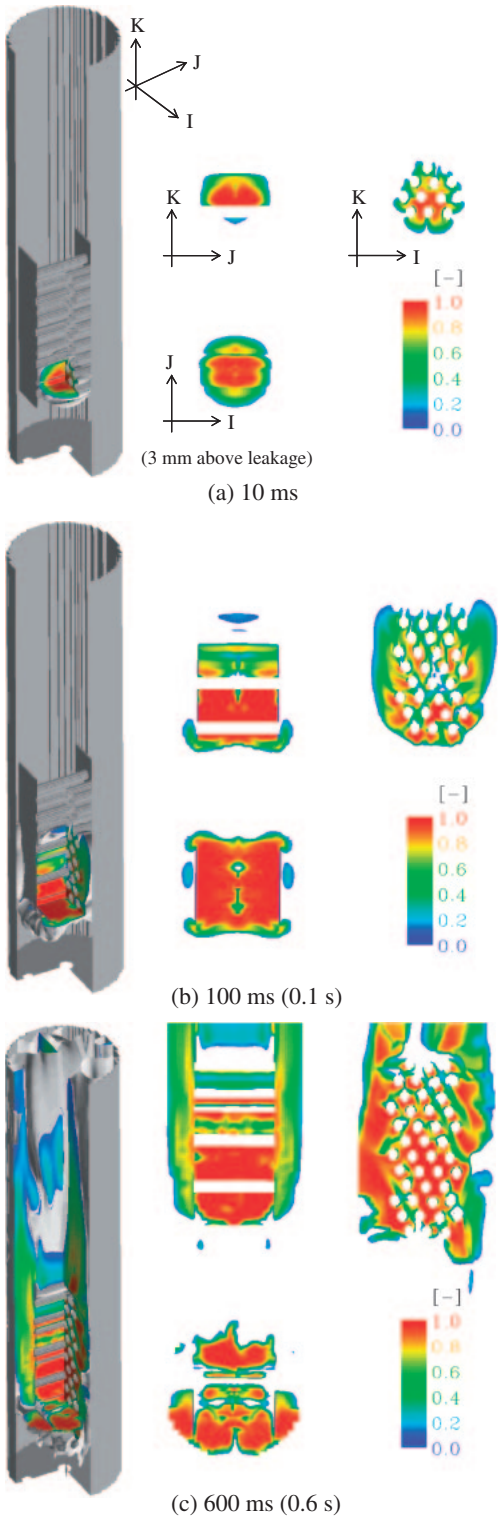

Fig. 5 Analytical result of gas volume (void) fraction

rated value. As a result, the leakage rate developed gradually in the experiment, and it took several seconds to obtain the constant leakage rate. However, the fully developed leakage rate shows excellent agreement between the analysis (0.162 kg/s) and the experiment (0.158 kg/s).

With regard to the pressure distribution, the pressure decreases rapidly from the leakage, and the critical jet flow of water vapor is formed in the computation. No significant

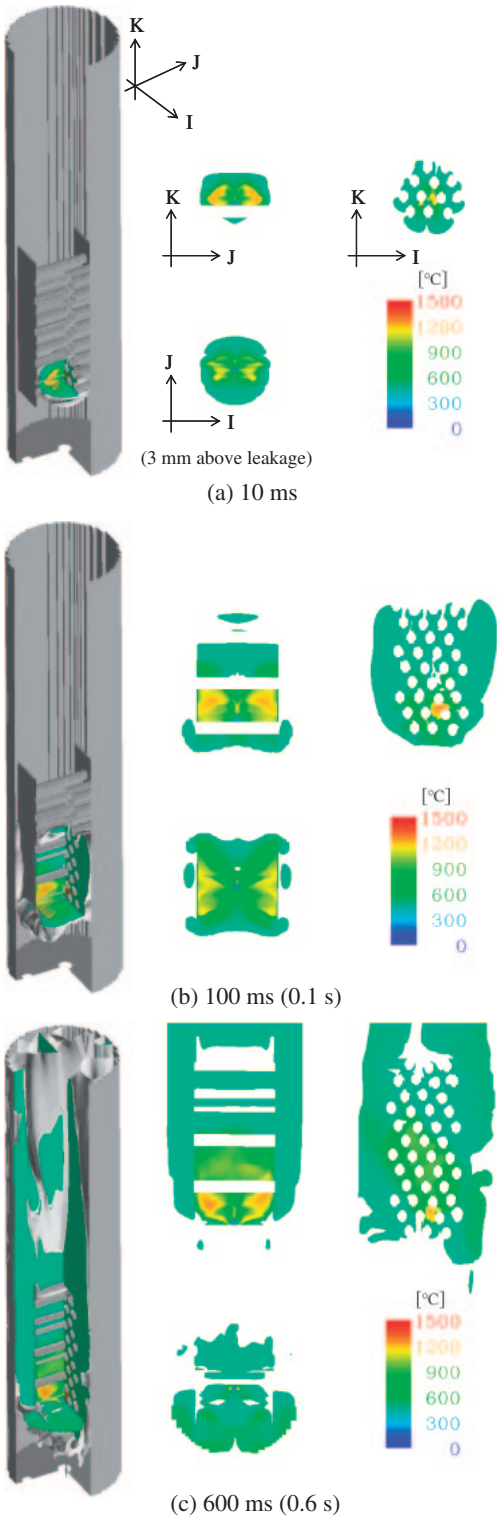

Fig. 6 Analytical result of gas temperature

pressure increase due to the highly pressurized water vapor at the leakage is found at the reacting zone.

The high-temperature region (over 1,000°C) reaches an adjoining tube even at an early stage of the analysis and surrounds the leakage, as seen in Fig. 6(a). This corresponds to the fact that the high-temperature region appears just near the interface between the water vapor and the liquid sodium owing to the surface reaction. As seen in Figs. 6(b) and 6(c),

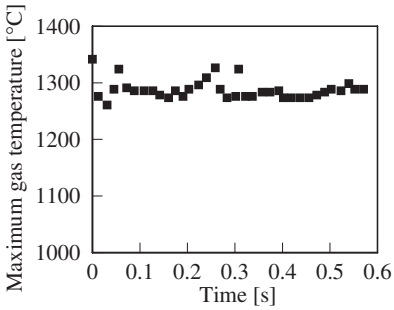

Fig. 7 Trend of maximum gas temperature

the longitudinal coverage of the high-temperature region in vertical axis seems not to be changed differently. Hence, it is said that the high-temperature region will develop well within a short period of time.

Figure 7 shows the trend of the maximum gas temperature during the analysis. The maximum value of approximately 1,300°C, which lies within the range of the previous experimental observations (1,095–1,371°C), is predicted constantly regardless of gas region development. The reason why the constant maximum value is predicted can be explained as follows.

The volume fractions of (a) water vapor and (b) hydrogen gas in the gas phase at 10 ms are depicted in **Fig. 8**. Comparing Fig. 8(a) with Fig. 6(a), it is again said that the high-temperature region exists just near the interface between the water vapor and the liquid sodium. At the same time, hydrogen gas produced at the interface covers up the interface, as in Fig. 8(b). Consequently, the concentration of the water vapor is lowered at the interface and the chemical reaction is moderated, resulting in the constant maximum gas temperature value regardless of the transient.

Another important factor affecting the maximum temperature is the evaporation of sodium hydroxide, as shown in Eqs. (12) and (13). **Figure 9** shows the volume fraction of the gas-phase sodium hydroxide at 10 ms. The gas-phase sodium hydroxide appears at the high-temperature region (see Fig. 6(a)). It is apparent that the total heat generation is reduced by the latent heat, resulting in a decrease in maximum temperature.

Figure 10 represents the comparison of the temperature distribution at the center of the bundle between the computation and the experiment. In the experiment, the average of thermocouples was taken three seconds after the leakage rate was almost kept constant. On the other hand, the mass weighted mean temperature of the gas and the liquid sodium at 0.6 s is drawn in the case of the computational result. It is noted that the red symbols on the right side of Fig. 10 reveals the locations of the thermocouples.

The high-temperature region develops along the inline direction both in the analysis and the experiment. The maximum value in the analysis agrees with the experimental result, whereas the high-temperature region is overestimated in the analysis. In the experiment, the reaction heat was removed from one tube by forced convection (see Fig. 2) and it would also be removed from the other tubes because

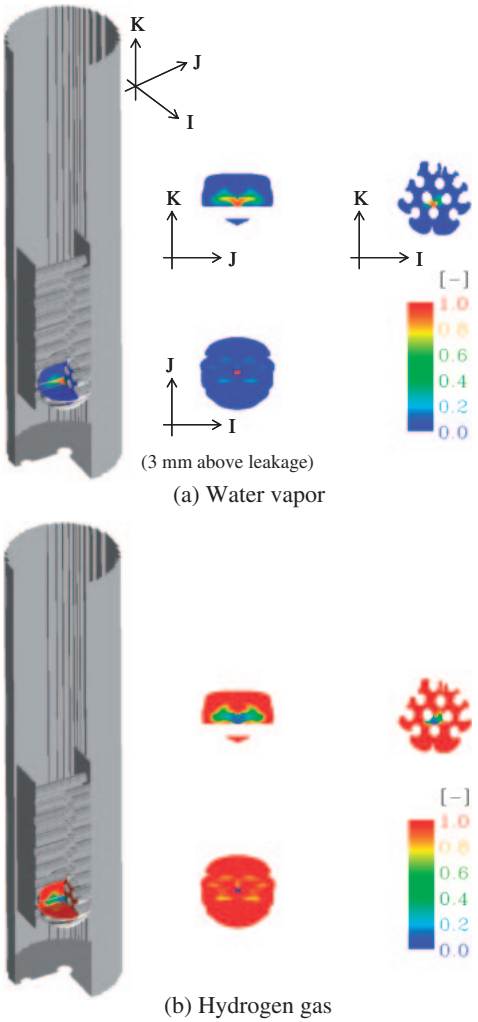

Fig. 8 Volume fraction in gas phase species at 10 ms

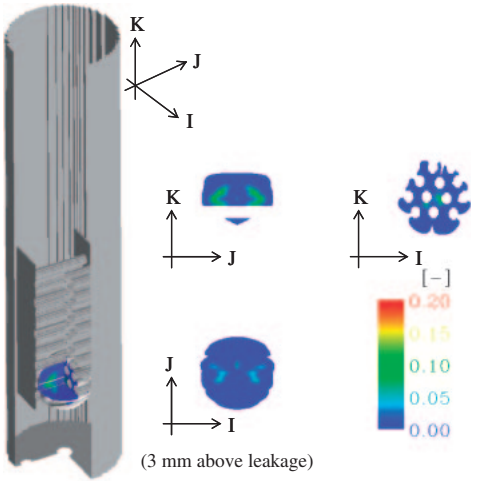

Fig. 9 Volume fraction of gas phase sodium hydroxide at 10 ms

both ends of the tube was opened. On the contrary, the tubes are treated as an adiabatic in the analysis. Therefore, the overestimation of the high-temperature region might be predicted in the analysis. With regard to the experimental results, it is also mentioned that the thermocouples placed in

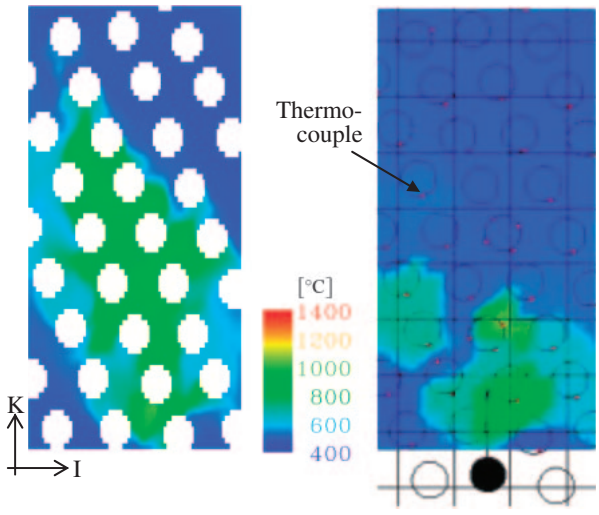

Fig. 10 Comparison of mean temperature at the center of the bundle

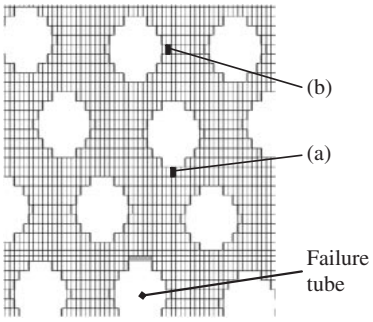

Fig. 11 Evaluation points

the test section are not sufficient to depict the temperature distribution in detail.

The characteristics of the reacting zone near the neighboring tubes play important roles in the secondary failure caused by the overheating rupture and wastage. Let us discuss the transient characteristics near the neighboring tubes. Two locations near the outer surface of surrounding tubes are chosen as examples. The locations of examples are depicted in **Fig. 11**.

Figure 12 shows the time transient of the temperature and the gas volume fraction in the analysis. The black solid and dashed lines indicate the temperatures of the gas phase and the liquid sodium, respectively, whereas the gray line shows the gas volume fraction. At position (a), the high-temperature gas reaches the neighbor tube continuously in a short period of time. The liquid sodium acts as a dispread phase and a thermal nonequilibrium state is investigated in almost the entire computational duration. On the other hand, the gas region fully develops after approximately 0.2 s at position (b). In addition, a thermal equilibrium state is almost achieved and a comparatively lower temperature is predicted than that in position (a). It might be said that the thermal equilibrium state is achieved quickly in the SWR phenomenon. It is noted that the upper limitation of the liquid sodium tem-

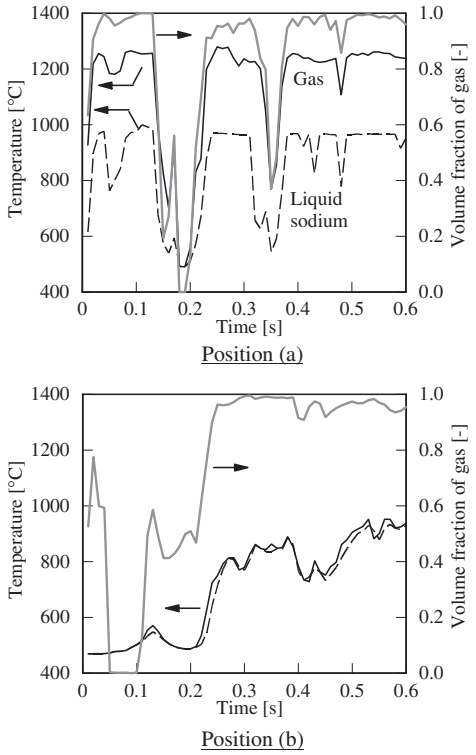

Fig. 12 Transient of gas volume fraction and temperature

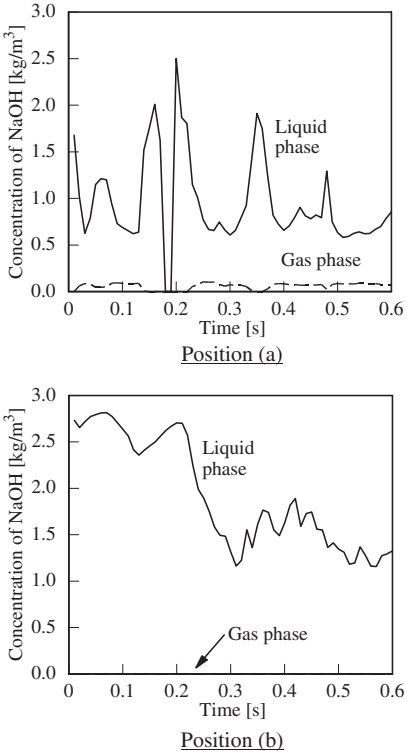

Fig. 13 Transient of sodium hydroxide concentration

perature seen at position (a) almost corresponds to the boiling point of liquid sodium at that pressure (approximately 0.2 MPa). It is noted that the nonequilibrium evaporation/condensation model[22] is implemented in the SERAPHIM code.

When one takes the overheating rupture into consideration, the quantification of heat transfer to a tube is essential rather than the evaluation of the maximum temperature near the tube. The authors have developed the quantification method of the heat transfer using one-dimensional thermal-hydraulic and structural analyses based on the boundary layer approximation.[28] Applying the present results shown in Fig. 12 to the quantification of the heat transfer, the possibility of the overheating rupture is to be evaluated in a future work.

Figure 13 depicts the numerical result of the mass concentration of sodium hydroxide at each location. Concerning the tube failure due to the wastage, a caustic environment in the reacting zone is important, as well as the temperature and velocity profiles. As shown in Fig. 13, the mass concentration of sodium hydroxide at position (b) is larger than that at position (a). This is because gas density increases in accordance with the decrease in temperature. Hence, it might be said that the higher erosive action occurs at position (b). On the contrary, the corrosive effect will be more intense at position (a) than at position (b) because of the higher temperature and the existence of the gas-phase sodium hydroxide.

Unfortunately, the theoretical and mechanistic modeling of the wastage, in which the local characteristics of the reacting zone are considered, has not matured well. This is attributed to the fact that the measurements, such as those of the temperature, velocity, and mass concentration of the product, are quite difficult in an actual SWR phenomenon. Accordingly, it is said that the numerical investigation near the surface of the neighboring tube is useful and helpful for the modeling of the wastage.

IV. Conclusions

The applicability of the SERAPHIM code to the complicated geometrical configuration is investigated. The SWAT-1R experiment, in which the sodium-water reaction (SWR) phenomenon was observed under a pin bundle of 43 heat transfer tubes, is chosen as the benchmark problem.

As a result, it is demonstrated that good agreements are obtained in terms of leakage rate and mass weighted average temperature, although the high-temperature region ($>$1,000°C) is overestimated in the computation. In the experiment, the reaction heat was removed from one heat transfer tube in which a forced convection using liquid sodium was done. On the other hand, the adiabatic condition is applied to the inner structure in the analysis. Therefore, the overestimation would be predicted in the analysis. It will be said that the SWR with a complicated structural configuration can be investigated using the SERAPHIM code.

In the analysis, the maximum temperature of approximately 1,300°C is predicted constantly during the analysis because hydrogen gas covers the interface between the water vapor and the liquid sodium where the SWR is most intense. It is also demonstrated that evaporation of sodium hydroxide suppresses the increase in the maximum temperature.

From the viewpoint of the structural integrity in a steam generator of sodium-cooled fast reactor, a secondary failure due to an overheating rupture and a wastage is of great concern. It is concluded that the present methodology (SERAPHIM code) is promising for evaluating a heat transfer to the neighboring tube and a possibility of the overheating rupture. The numerical quantification of the heat transfer and the possibility of the overheating rupture will be carried out in a future work. It is also mentioned that the present methodology is useful and helpful to develop a theoretical and mechanistic modeling of the wastage phenomena.

Nomenclature

a: interfacial area density [1/m]
b: empirical constants [—]
Cp: specific heat at constant pressure [J/kg/K]
f^{ph}: interfacial friction coefficient [Ns/m^4]
f^{w}: wall friction coefficient [Ns/m^4]
G: leakage rate [g/s]
$\boldsymbol{g}$: gravity vector [m/s^2]
H: heat transfer coefficient [W/m^2/K]
h: enthalpy [J/kg]
hy: enthalpy of gas component [J/kg]
i: latent heat [J/kg]
i_{st}: stoichiometric coefficient [—]
$k(T)$: rate constant [mol, m, s]
L: distance between leakage and target [mm]
Le: Lewis number [—]
M: molar weight [kg/mol]
p: pressure [Pa]
R: gas constant [J/mol/K]
T_S: sodium temperature [K]
t: time [s]
$\mathbf{u}$: velocity vector [m/s]
W_R: wastage rate [mm/s]
Y: mass fraction of gas species [—]

Greek Letters

α: volume fraction [—]
$\Delta H^0{}_{298}$: standard enthalpy change of formation [J/mol]
Δt: time step [s]
Φ: dissipation function [W/m^3]
Γ^c: condensation rate [kg/m^3/s]
Γ^e: evaporation rate [kg/m^3/s]
γ: reaction rate [kg/m^3/s]
λ: thermal conductivity [W/m/K]
ρ: density [kg/m^3]
$\boldsymbol{\tau}$: viscous stress tensor [N/m^2]
ω: relaxation factor [—]

Superscripts

sf: surface reaction
gs: gas-phase reaction
dif: diffusive term due to Dufour effect

Subscripts

g: gas phase
H_2O: water vapor
S: liquid sodium
H: water

References

1) H. Hori, "Sodium/water reactions in steam generators of liquid metal fast breeder reactors," *At. Energ. Rev.*, **18**[3], 707–778 (1980).
2) H. H. Neely, C. E. Boardman, "Status of U.S. studies of failures and failure propagation in steam generator," *Proc. IAEA/IWGFR Specialists' Meeting on Steam Generator Failure and Failure Propagation Experience*, Aix-en-Provence, France, 24–35 (1990).
3) M. Mori, "Sodium/water reactions in steam generators of liquid metal fast breeder reactors," *At. Energ. Rev.*, **18**[3], 707–778 (1980).
4) O. Miyake, H. Hamada, H. Tanabe *et al.*, *The Development and Application of Overheating Failure Models of FBR Steam Generator Tube (IV)*, JNC TN2400 2003-003, Japan Nuclear Cycle Development Institute (JNC) (2003), [in Japanese].
5) H. Seino, I. Ono, H. Hamada, *Development of LEAP-JET Code for Sodium-Water Reaction Analysis—Validation by Sodium-Water Reaction Tests (SWAT-1R)—*, JNC TN9400 2003-106, Japan Nuclear Cycle Development Institute (JNC) (2003), [in Japanese].
6) T. Morii, Y. Ogawa, "Development and application of a fully implicit fluid dynamics code for multiphase flow," *Nucl. Technol.*, **115**, 333–341 (1996).
7) T. Takata, A. Yamaguchi, "Numerical approach to the safety evaluation of sodium-water reaction," *J. Nucl. Sci. Technol.*, **40**[10], 708–718 (2003).
8) T. Takata, A. Yamaguchi, K. Fukuzawa, K. Matsubara, "Numerical methodology of sodium-water reaction with multiphase flow analysis," *Nucl. Sci. Eng.*, **150**, 221–236 (2005).
9) T. Takata, A. Yamaguchi, H. Ohshima, A. Watanabe, "Computational sensitivity study on sodium-water reaction phenomenon," *J. Nucl. Sci. Technol.*, **43**[5], 514–525 (2006).
10) M. Nishimura, K. Shimoyama *et al.*, *Sodium-Water Reaction Test to Confirm Thermal Influence on Heat Transfer Tubes*, JNC TN9400 2003-014, Japan Nuclear Cycle Development Institute (JNC) (2003), [in Japanese].
11) R. N. Newman, A. R. Pugh, C. A. Smith, "Explosive interaction between sodium and water, and material wastage in the vicinity of leaks in sodium water heat exchanges," *Liquid Alkali Metals*, The British Nuclear Energy Society, London, 85–91 (1973).
12) International Atomic Energy Agency, *Fast Reactor Fuel Failures and Steam Generator Leaks: Transient and Accident Analysis Approaches*, IAEA-TECDOC-908 (1996).
13) Y. Okano, A. Yamaguchi, "Numerical simulations study on sodium-water reaction. (4) Theoretical adiabatic temperature of sodium-water reaction zone," *2001 Annual Meeting of AESJ*, I4 (2001), [in Japanese].
14) H. Tanabe, Y. Wada, K. Hamada *et al.*, *The Development and Application of Overheating Failure Model of FBR Steam Generator Tubes*, PNC TN9410 98-029, Japan Nuclear Cycle Development Institute (JNC) (1998), [in Japanese].
15) T. Takata, A. Yamaguchi, A. Watanabe, *Modification of Multi-dimensional Sodium-Water Reaction Analysis Code: SERAPHIM and Sensitivity Analyses on the Early Stage of Leakage*, JNC TN9400 2003-024, Japan Nuclear Cycle Development Institute (JNC) (2003), [in Japanese].
16) M. J. Pilling, *Reaction Kinetics*, Clarendon Press, Oxford (1974).
17) E. Herbst, *Atomic Molecular and Optical Physics Reference Book*, G. Drake (New York: AIP), 429 (1996).
18) M. Benedict, G. B. Webb, L. C. Rubin, "An empirical equation for thermodynamic properties of light hydro-carbons and their mixtures," *J. Chem. Phys.*, **8**, 344 (1940).
19) T. Takata, A. Yamaguchi, A. Hashimoto, *Development of Multi Components and Multi Phase Numerical Method with*

Chemical Reaction, JNC TN9400 2001-125, Japan Nuclear Cycle Development Institute (JNC) (2001), [in Japanese].
20) W. C. Rivard, M. D. Torrey, *Numerical Calculation of Flashing from Long Pipes Using a Two-Field Model*, LASM LAMS-NUREG-6330 (1976).
21) H. Ninokata, T. Okano, "SABENA: An advanced subchannel code for sodium boiling analysis," *Proc. 3rd Int. Mtg. on Reactor Thermal Hydraulics*, Newport, Oct., 16.K (1985).
22) R. Takahashi, A. Tomiyama, "Consideration on computational method of two-phase flow problem," *J. AESJ*, **26**[11], 988 (1984), [in Japanese].
23) R. C. Martinelli, D. B. Nelson, "Prediction of pressure drop during forced circulation boiling of water," *Trans. ASME*, **70**, 695 (1948).
24) J. Gullbrand, F. K. Chow, "The effect of numerical errors and turbulence models in large-eddy simulations of channel flow, with and without explicit filtering," *J. Fluid Mech.*, **495**, 323–341 (2003).
25) M. Nishimura, K. Shimoyama *et al.*, *Sodium-Water Reaction Test to Confirm Thermal Influence on Heat Transfer Tubes*, JNC TN9400 2003-014, Japan Nuclear Cycle Development Institute (JNC) (2003), [in Japanese].
26) H. Tanabe, T. Watanabe, *Results of Failure Propagation Tests in the Steam Generator Safety Facility (SWAT-3) Report No. 5*, PNC SN9410 86-104, Power Reactor and Nuclear Fuel Development Corporation (PNC) (1986), [in Japanese].
27) M. W. Chase, Jr., C. A. Davies *et al.*, *JANAF Thermochemical Tables Third Edition Part II, Cr-Zr*, American Institute of Physics, Inc., New York (1986).
28) A. Yamaguchi, Y. Tajima *et al.*, "Numerical simulation study on sodium water reaction (11) evaluation of sodium-tube heat transfer coefficient based on numerical simulation and experiment," *2004 Annual Meeting of AESJ*, M14 (2004), [in Japanese].